

Electronic Supporting Information

Room temperature phosphorescence in longer-wavelength red light region found in benzothiadiazole-based dyes

Tsutomu Ishi-i,^{*a} Rihoko Kichise,^{a,b} In Seob Park,^c Takuma Yasuda,^c and Taisuke Matsumoto^d

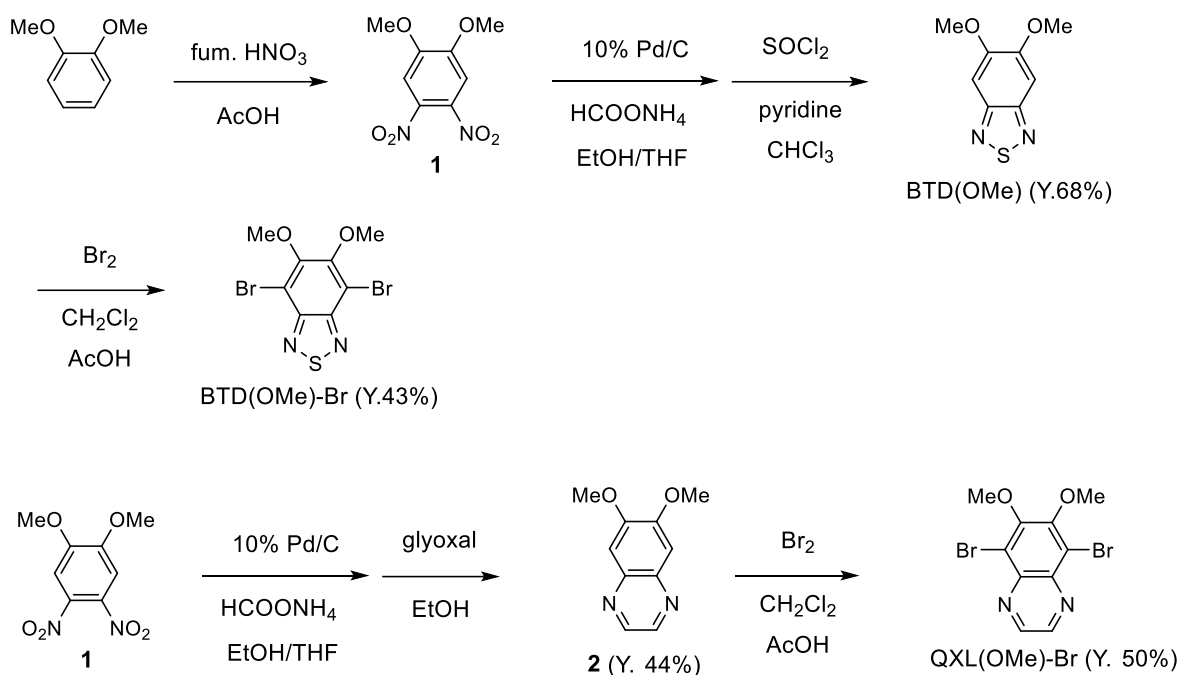
Table of Contents

Experimental section	2–6
Absorption and fluorescence spectra in solution: Figs. S1–S3 and Table S1	7–8
Photoluminescence, excitation and diffuse reflection spectra in the solid state: Figs. S4–S11	9–12
Fluorescence and phosphorescence lifetime: Figs. S12 and S13	13
Spectral data in the solid state: Tables S2 and S3	14–16
Differential scanning calorimetry: Fig. S14	17
Powder X-ray diffraction measurement: Figs. S15 and S16	18
Computer simulation analysis: Figs. S17 and S18	19–21
Single crystal X-ray diffraction analysis: Figs. S19 and S20, and Tables S4 and S5	22–26
¹ H and ¹³ C NMR spectra of new compounds; Figs. S21–S28	27–30

Experimental Section

General. All melting points are uncorrected. IR spectra were recorded on a JASCO FT/IR-470 plus Fourier transform infrared spectrometer, and measured on KBr pellets. ^1H and ^{13}C NMR spectra were determined in CDCl_3 with a JEOL ECX 500 spectrometer. Residual solvent protons were used as internal standard and chemical shifts (δ) are given relative to tetramethylsilane (TMS). The coupling constants (J) are reported in hertz (Hz). Elemental analysis was performed at the Elemental Analytical Center, Kyushu University. Fast atom bombardment mass spectrometry (FAB-MS) spectra were recorded with a JEOL JMS-70 mass spectrometer with m-nitrobenzyl alcohol (NBA) as a matrix. Gel permeation chromatography (GPC) was performed with a Japan Analytical Industry LC-908 using JAIGEL-1H column (20×600 mm) and JAIGEL-2H column (20×600 mm) eluting with chloroform (3.0 mL/min). Analytical TLC was carried out on silica gel coated on aluminum foil (Merck 60 F254). Column chromatography was carried out on silica gel (WAKO C300). Dry THF was purchased from FUJIFILM Wako Pure Chemical Corporation. Dichloromethane and acetic acid were dried over 4A molecular sieves and 3A molecular sieves, respectively, over night before use. 1,2-Dimethoxy-4,5-dinitrobenzene (**1**)¹ and 5,6-dimethoxy-2,1,3-benzothiadiazole (BTD(OMe))² were prepared according to the methods reported previously. 4,7-Dibromo-2,1,3-benzothiadiazole (BTD-Br), which was purchased from Tokyo Chemical Industry, was characterized after recrystallization from boiling butanol. 4,7-Dibromo-5,6-difluoro-2,1,3-benzothiadiazole (BTD(F)-Br), which was purchased from Sigma-Aldrich, was characterized after recrystallization from boiling hexane.

1. J. L. Sessler, W. B. Callaway, S. P. Dudek, R. W. Date and D. W. Bruce, *Inorg. Chem.*, 2004, **43**, 6650–6653.
2. J. Hu, D. Zhang, S. Jin, S. Z. D. Cheng and F. W. Harris, *Chem. Mater.*, 2004, **16**, 4912–4915; J. Bouffard and T. M. Swager, *Macromolecules*, 2008, **41**, 5559–5562.



5,6-Dimethoxy-2,1,3-benzothiadiazole (BTD(OMe)). To a suspension of **1**¹ (2.35 g, 10.3 mmol) and 10% Pd/C (470 mg) in dry THF (30 mL) and deaerated ethanol (103 mL) was added portionwise ammonium formate (18.0 g, 285 mmol) and the mixture was stirred at room temperature for 1.5 h under an argon atmosphere. The reaction mixture was filtered over celite and wash with deaerated ethanol. The filtrate was evaporated in vacuo to dryness. Without further purification, the crude diamine derivative (4.38 g) was used to the next reaction. To a mixture of the diamine derivative (4.38 g) and pyridine (2.49 mL, 30.9 mmol) in deaerated chloroform (62 mL) was added dropwise thionyl chloride (3.80 g, 31.9 mmol) in deaerated chloroform (10 mL) at 0 °C for 6 min. The mixture was heated at the refluxing temperature for 2 h under an argon atmosphere. After the reaction mixture cooled to room temperature, it was quenched by addition of 1 M sodium hydrogen carbonate aqueous solution (100 mL) and acidified by addition of 1.2 M hydrochloric acid aqueous solution (pH 4~5). The resulting mixture was extracted with chloroform. The combined organic layer was washed with brine and water, dried over anhydrous magnesium sulfate, and evaporated in vacuo to dryness. The residue was purified by silica gel column chromatography (WAKO C300) eluting with hexane/chloroform (1:2, v/v) to give BTD(OMe) in 68% (1.38 g, 7.03 mmol). An analytical sample was obtained by recrystallization from hexane/chloroform as colorless needles: mp 160–161 °C; IR (KBr, cm⁻¹) 3067, 3038, 2940, 2836, 1493, 1435,

1306, 1215, 1168, 1010, 843, 839, 813, 756, 661, 617; ^1H NMR (CDCl_3 , 500 MHz) δ 4.01 (s, 6 H, CH_3), 7.19 (s, 2 H, Ar); ^{13}C NMR (CDCl_3 , 126 MHz) δ 56.35, 97.98, 151.28, 154.24; FAB-MS (positive, NBA) m/z 197 $[(\text{M}+1)^+]$. Anal. Calcd for $\text{C}_8\text{H}_8\text{N}_2\text{O}_2\text{S}$ (196.23): C, 48.97; H, 4.11; N, 14.28. Found: C, 48.82; H 4.21; N, 14.05.

4,7-Dibromo-5,6-dimethoxy-2,1,3-benzothiadiazole (BTD(OMe)-Br). To a solution of BTD(OMe) 2 (1.01 g, 5.13 mmol) in dry dichloromethane (128 mL) and acetic acid (62 mL) was added bromine (5.0 g, 31.4 mmol) in dichloromethane (5 mL) under an argon atmosphere and the mixture was stirred at room temperature for 24 h under dark conditions. After the reaction mixture was quenched by addition of cold water and 1 M aqueous solution of sodium hydrogen sulfite, it was extracted with chloroform. The combined organic layer was washed with 1 M aqueous solution of sodium hydrogen sulfite and water, dried over anhydrous magnesium sulfate, and evaporated in vacuo to dryness. The residue was purified by silica gel column chromatography (WAKO C300) eluting with hexane/chloroform (1:1, v/v) to give BTD(OMe)-Br in 43% yield (786 mg, 2.22 mmol). An analytical sample was obtained by recrystallization from hexane/chloroform as colorless needles: mp 132–133 °C; IR (KBr, cm^{-1}) 3019, 2989, 2946, 2882, 2859, 1457, 1406, 1285, 1264, 1044, 976, 881, 818; ^1H NMR (CDCl_3 , 500 MHz) δ 4.05 (s, 6 H, CH_3); ^{13}C NMR (CDCl_3 , 126 MHz) δ 61.62, 106.14, 150.30, 154.82; FAB-MS (positive, NBA) m/z 353, 355, 357 $[(\text{M}+1)^+]$. Anal. Calcd for $\text{C}_8\text{H}_6\text{Br}_2\text{N}_2\text{O}_2\text{S}$ (354.02): C, 27.14; H, 1.71; N, 7.91. Found: C, 27.13; H 1.76; N, 7.81.

6,7-Dimethoxyquinoxaline (2). To a suspension of **1** (1.14 g, 5.0 mmol) and 10% Pd/C (228 mg) in dry THF (15 mL) and deaerated ethanol (50 mL) was added portionwise ammonium formate (8.7 g, 138 mmol) and the mixture was stirred at room temperature for 2 h under an argon atmosphere. The reaction mixture was filtered over celite and wash with deaerated ethanol. The filtrate was evaporated in vacuo to dryness. Without further purification, the crude diamine derivative (1.85 g) was used to the next reaction. A mixture of the diamine derivative (1.85 g) and 8.8 M aqueous glyoxal solution (0.57 mL, 5.0 mmol) in deaerated ethanol (34 mL) was heated at the refluxing temperature for 7 h under an argon atmosphere. After the reaction mixture cooled to room temperature, it was distilled under reduced pressure (ca. 40 torr) to remove most of ethanol. The

resulting mixture was poured into water and extracted with chloroform. The combined organic layer was washed with brine and water, dried over anhydrous magnesium sulfate, and evaporated in vacuo to dryness. The residue was purified by silica gel column chromatography (WAKO C300) eluting with dichloromethane/methanol (49:1, v/v) to give **2** in 44% yield (423 mg, 2.2 mmol). An analytical sample was obtained by recrystallization from hexane/dichloromethane as colorless needles: mp 154–155 °C; IR (KBr, cm^{-1}) 3063, 3006, 2967, 2942, 2879, 2847, 2822, 1619, 1501, 1476, 1439, 1420, 1310, 1254, 1210, 1137, 1046, 1006, 868; ^1H NMR (CDCl_3 , 500 MHz) δ 4.07 (s, 6 H, CH_3), 7.36 (s, 2 H, ArH), 8.65 (s, 2 H, ArH); ^{13}C NMR (CDCl_3 , 126 MHz) δ 56.33, 106.76, 140.33, 142.46, 152.83; FAB-MS (positive, NBA) m/z 191 $[(\text{M}+1)^+]$. Anal. Calcd for $\text{C}_{10}\text{H}_{10}\text{N}_2\text{O}_2$ (190.20): C, 63.15; H, 5.30; N, 14.73. Found: C, 63.16; H, 5.26; N, 14.70.

5,8-Dibromo-6,7-dimethoxyquinoxaline (QXL(OMe)-Br). To a solution of **2** (380 mg, 2.0 mmol) in dry dichloromethane (50 mL) and acetic acid (24 mL) was added bromine (1.28 g, 8.0 mmol) in dichloromethane (2 mL) under an argon atmosphere and the mixture was stirred at room temperature for 24 h under dark conditions. After the reaction mixture was quenched by addition of cold water and 1 M aqueous solution of sodium hydrogen sulfite, it was extracted with chloroform. The combined organic layer was washed with 1 M aqueous solution of sodium hydrogen sulfite and water, dried over anhydrous magnesium sulfate, and evaporated in vacuo to dryness. The residue was purified by silica gel column chromatography (WAKO C300) eluting with dichloromethane to give QXL(OMe)-Br in 50% (348 mg, 1.0 mmol). An analytical sample was obtained by recrystallization from hexane/dichloromethane as colorless needles: mp 188–189 °C; IR (KBr, cm^{-1}) 3042, 2997, 2972, 2937, 2861, 2836, 1466, 1401, 1351, 1330, 1128, 1055, 991, 945, 870, 758; ^1H NMR (CDCl_3 , 500 MHz) δ 4.09 (s, 6 H, CH_3), 8.92 (s, 2 H, Ar); ^{13}C NMR (CDCl_3 , 126 MHz) δ 61.44, 117.22, 139.41, 144.73, 154.53; FAB-MS (positive, NBA) m/z 347, 349, 351 $[(\text{M}+1)^+]$. Anal. Calcd for $\text{C}_{10}\text{H}_8\text{Br}_2\text{N}_2\text{O}_2$ (347.99): C, 34.51; H, 2.32; N, 8.05. Found: C, 34.71; H, 2.21; N, 8.00.

Instrumentation. Steady-state photoluminescence spectra and excitation spectra were measured on a JASCO FP-8600 fluorescence spectrophotometer. Absorption spectra were measured on a JASCO V-570

spectrophotometer. Diffuse reflection spectra were measured on a JASCO V-670 spectrophotometer equipped with a JASCO ISV-922 integrating sphere system. A film sample for the photoluminescence spectral measurement was prepared by drop casting and subsequent spin-coating (2000 rpm, 30 s) from PMMA dichloromethane solution including 0.5 wt.-% BTD(OMe)-Br molecule. The fluorescence and phosphorescence quantum yield were measured with an absolute photoluminescence quantum yield measurement system (Hamamatsu Photonics, Quantaury-QY C11347-01). This instrument consisted of an integrating sphere equipped with a monochromatized Xe arc lamp as the light source and a multichannel spectrometer. The sensitivity of this system was fully calibrated using deuterium and halogen standard light sources. Fluorescence lifetime measurements were made by using a laser diode (340 nm, pulse width 100 ps, repetition rate 20 kHz) and as the excitation light source and a time-correlated single-photon counting fluorometer (Hamamatsu Photonics, Quantaury-Tau C11367). For phosphorescence lifetime measurements, a LED diode (340 nm, pulse width 1 ns, repetition rate 2 kHz) was used as the excitation light source. The analysis of the fluorescence and phosphorescence decay curves were carried out using the deconvolution method. Differential scanning calorimetry was performed on a METTLER TOLEDO DSC822e at heating and cooling rates of 10 K min⁻¹ under a nitrogen atmosphere. Powder X-ray diffraction measurements were performed on RIGAKU RINT-TTR III and carried out with Cu(K α) radiation from an X-ray tube with a 0.5 \times 10 mm² filament operated at 50 kV \times 300 mA (15 kW).

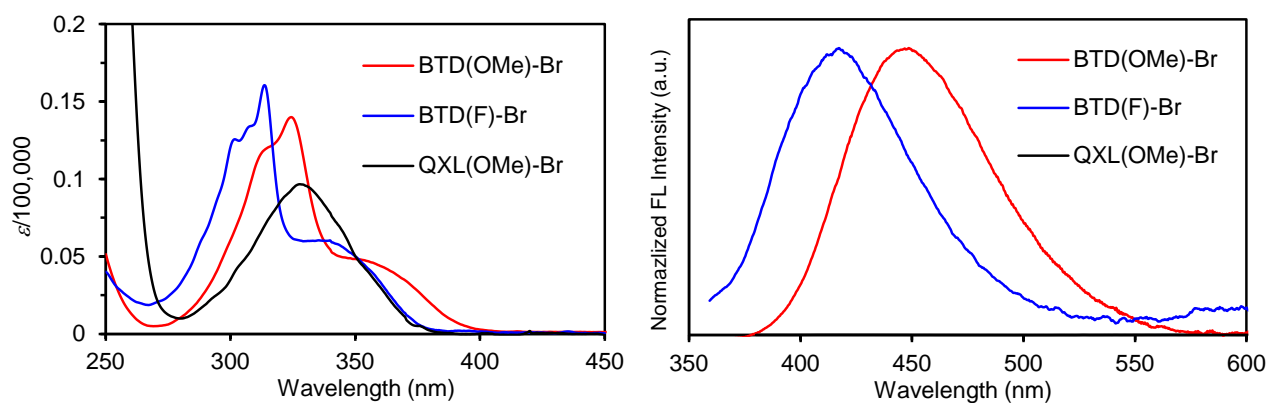


Fig. S1 UV/Vis absorption spectra and fluorescence spectra (ex. 325, 315, and 330 nm) of BTD(OMe)-Br, BTD(F)-Br, and QXL(OMe)-Br in DCM (1.0×10^{-5} M).

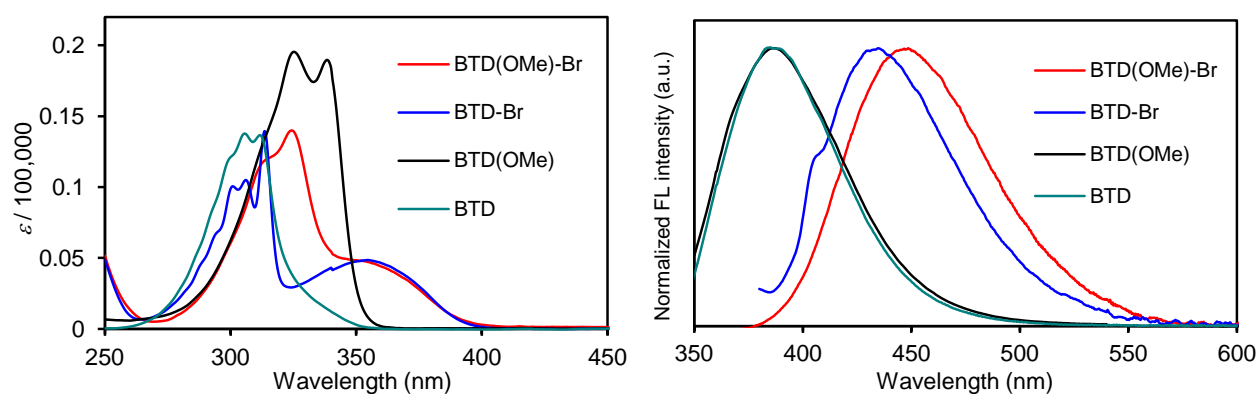


Fig. S2 UV/Vis absorption spectra and fluorescence spectra (ex. 325, 360, 330, and 310 nm) of BTD(OMe)-Br, BTD-Br, BTD(OMe), and BTD in DCM ($1.0\sim 2.0 \times 10^{-5}$ M).

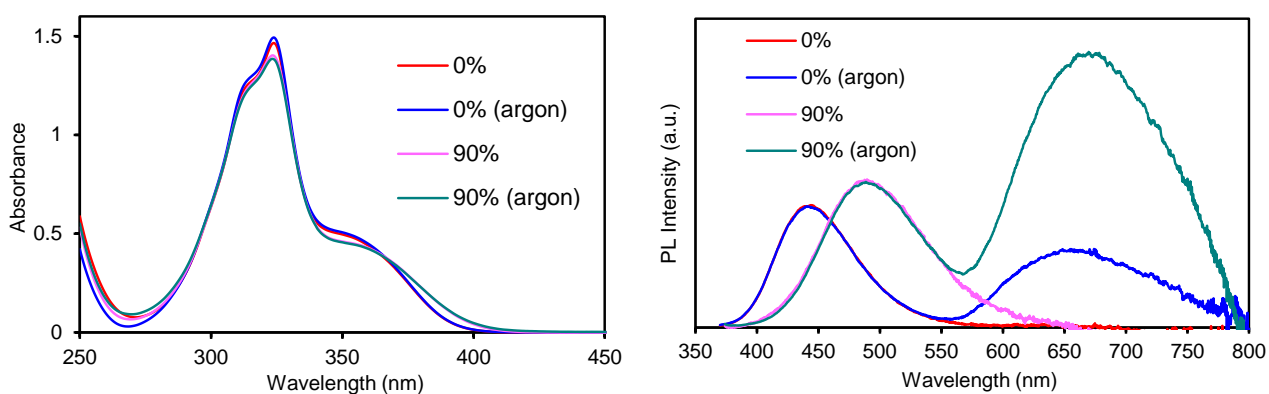


Fig. S3 UV/Vis absorption and photoluminescence (ex. 325 nm) spectra of BTD(OMe)-Br in THF/water (1×10^{-4} M: water fraction of 0 and 90%) at room temperature under air and argon atmosphere.

Table S1. Spectral data of benzothiadiazole-based dyes in solutions ^a

Comp.	Solvent	λ_{abs} (nm)	ϵ	ex (nm)	λ_{em} (nm)	Φ_{F} (%) ^c	Φ_{P} (%) ^c
BTD(OMe)-Br	DCM	363 (sh)	4,148	325	448	0.02	
		324	14,450				
	THF	360 (sh)	4,400	325	444	0.02	
		324	14,650				
	THF (Ar)	360 (sh)	4,490	325	644	0.02	0.02
		324	14,930		444		
	THF/water (90%) ^b	360 (sh)	4,290	325	488	0.02	
		324	14,040				
	THF/water (90%) (Ar) ^b	360 (sh)	4,080	325	670	0.02	0.05
324		13,850	489				
THF (77 K)	–	–		325	658 (sh)	0.04	2.4
					647		
					638		
					626 (sh)		
					598 (sh)		
					425		
BTD(F)-Br	DCM	340 (sh)	6,030	315	417	0.03	
		314	16,050				
QXL(OMe)-Br	DCM	328	9,660	330	<i>d</i>	<i>d</i>	
BTD-Br	DCM	355	4,860	360	435	1.1	
		314	13,940				
BTD(OMe)	DCM	339	18,970	330	387	4.4	
		325	19,540				
BTD	DCM	316	13,660	310	385	0.51	
		306	13,770				

^a 1×10^{-5} M, ^b 1×10^{-4} M, ^c Determined relative to Quinine sulfate (Φ_{FL} 0.55, ex 350 nm) in sulfuric acid,

^d Emission could not be detected.

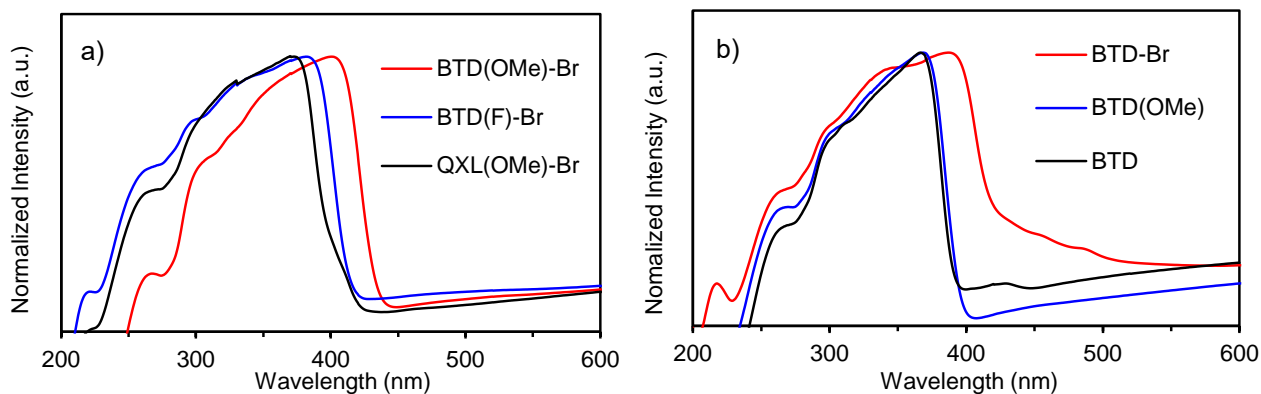


Fig. S4 Diffuse reflection UV/Vis spectra in the crystalline solid state for (a) BTD(OMe)-Br, BTD(F)-Br, and QXL(OMe)-Br and (b) BTD-Br, BTD(OMe), and BTD.

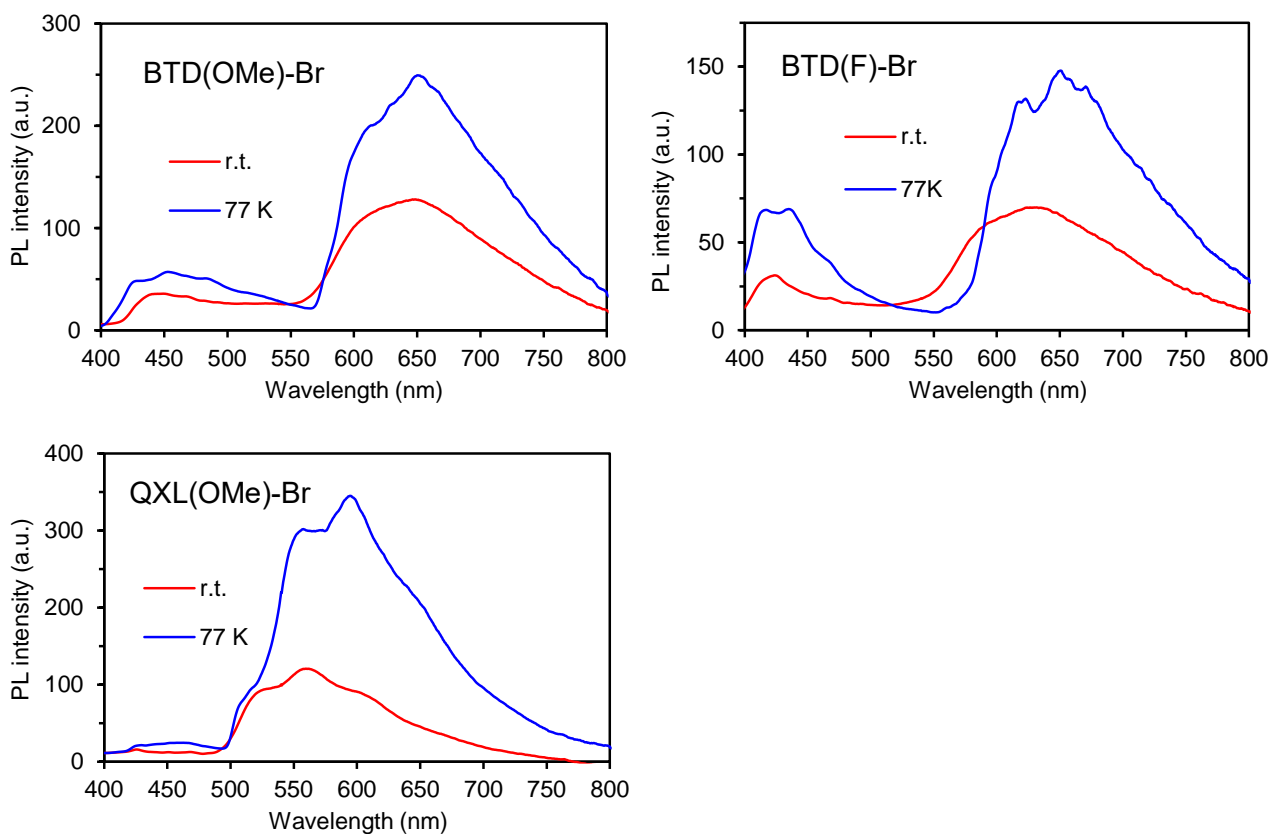


Fig. S5 Steady-state photoluminescence spectra (ex. 325 nm) of BTD(OMe)-Br, BTD(F)-Br, and QXL(OMe)-Br in the crystalline solid state at room temperature and 77 K.

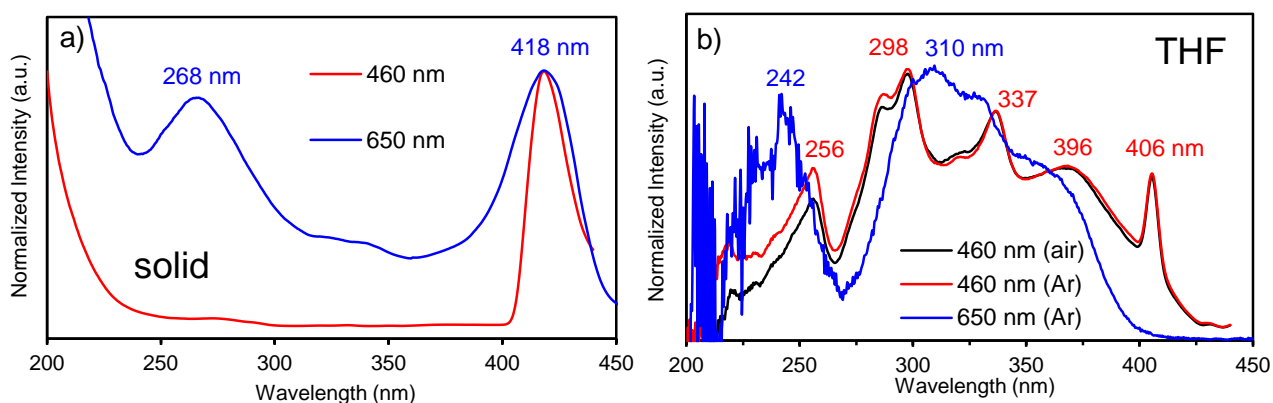


Fig. S6 Excitation spectra of BTDO(OMe)-Br monitored at 460 and 650 nm (a) in the crystalline solid state and (b) in THF (1×10^{-4} M) under air and argon atmosphere.

In the crystalline solid state, the excitation spectral data is likely to support the intersystem crossing, starting from the higher-lying excited singlet. The monitoring of fluorescence emission at 460 nm produces only a longer-wavelength excitation band at 418 nm, which is attributed to the transition from the ground state to the lowest excited singlet state. In addition to this longer-wavelength excitation band, a shorter-wavelength band at 268 nm is obtained by monitoring the phosphorescence emission at 650 nm. This shorter-wavelength band is attributed to the transition to a higher-lying excited singlet.

In THF, the intersystem crossing is likely to start from the higher-lying excited singlet, although different excitation spectral data was provided compared to the solid state. The emission band at 406 nm, which is attributed to the transition from the ground state to the lowest excited singlet state, was observed by monitoring of fluorescence emission at 460 nm. This excitation band disappeared by monitoring the phosphorescence emission at 650 nm, suggesting the intersystem crossing starting from the higher-lying excited singlet.

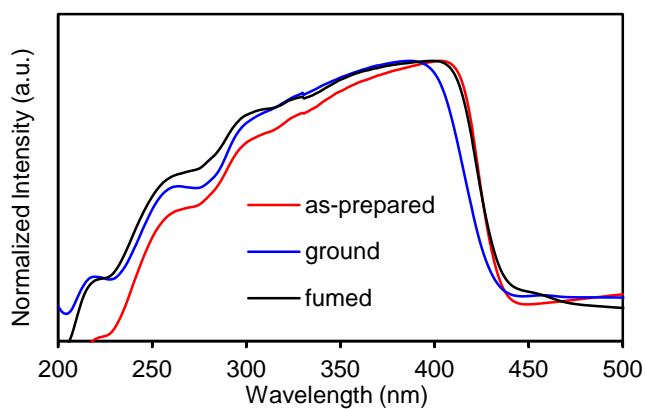


Fig. S7 Diffuse reflection UV/Vis spectra of the as-prepared, ground, and fumed (chloroform-vapor) samples of BTD(OMe)-Br in the solid state.

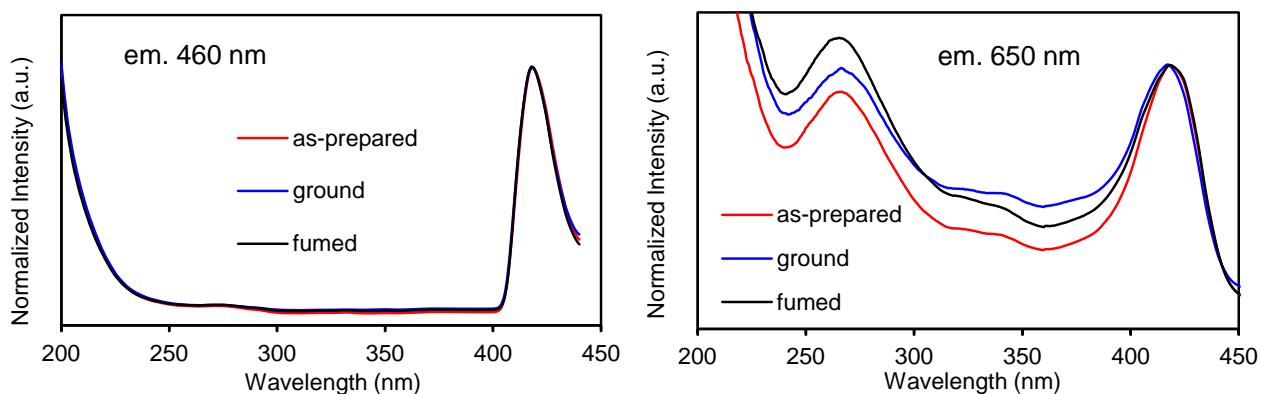


Fig. S8 Excitation spectra (monitored at 460 and 650 nm) of the as-prepared, ground, and fumed (chloroform-vapor) samples of BTD(OMe)-Br in the solid state.

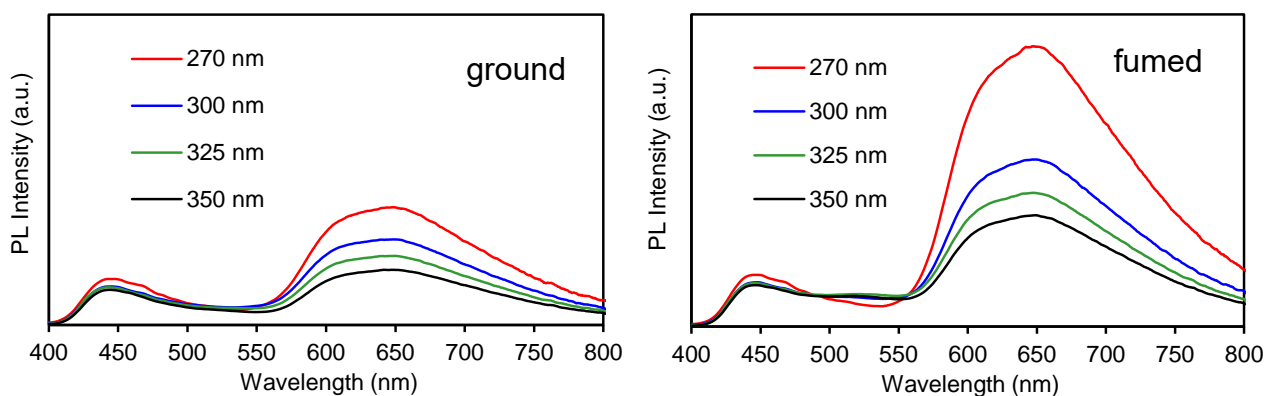


Fig. S9 Excitation dependence of steady-state photoluminescence spectra (excited at 270, 300, 325, and 350 nm) of the ground and fumed (chloroform-vapor) samples of BTD(OMe)-Br in the solid state.

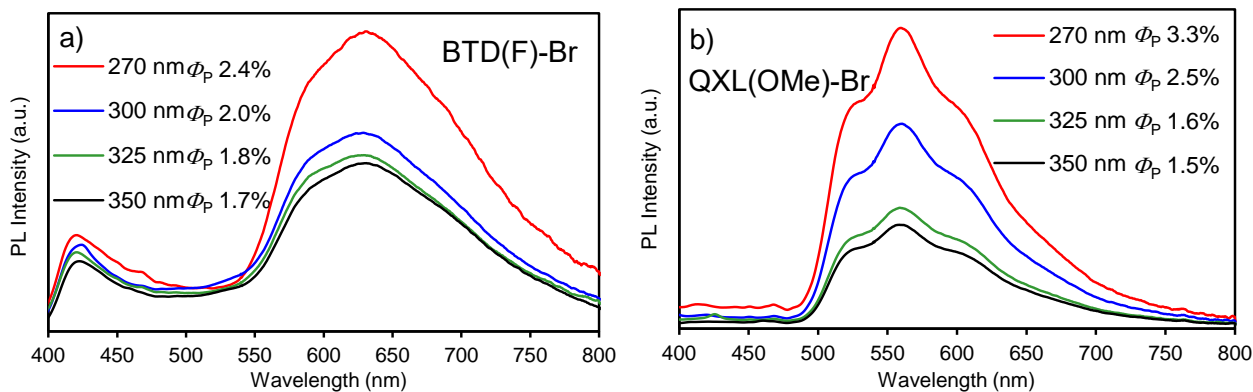


Fig. S10 Excitation dependence of steady-state photoluminescence spectra (excited at 270, 300, 325, and 350 nm) of (a) BTD(F)-Br and (b) QXL(OMe)-Br in the crystalline solid state.

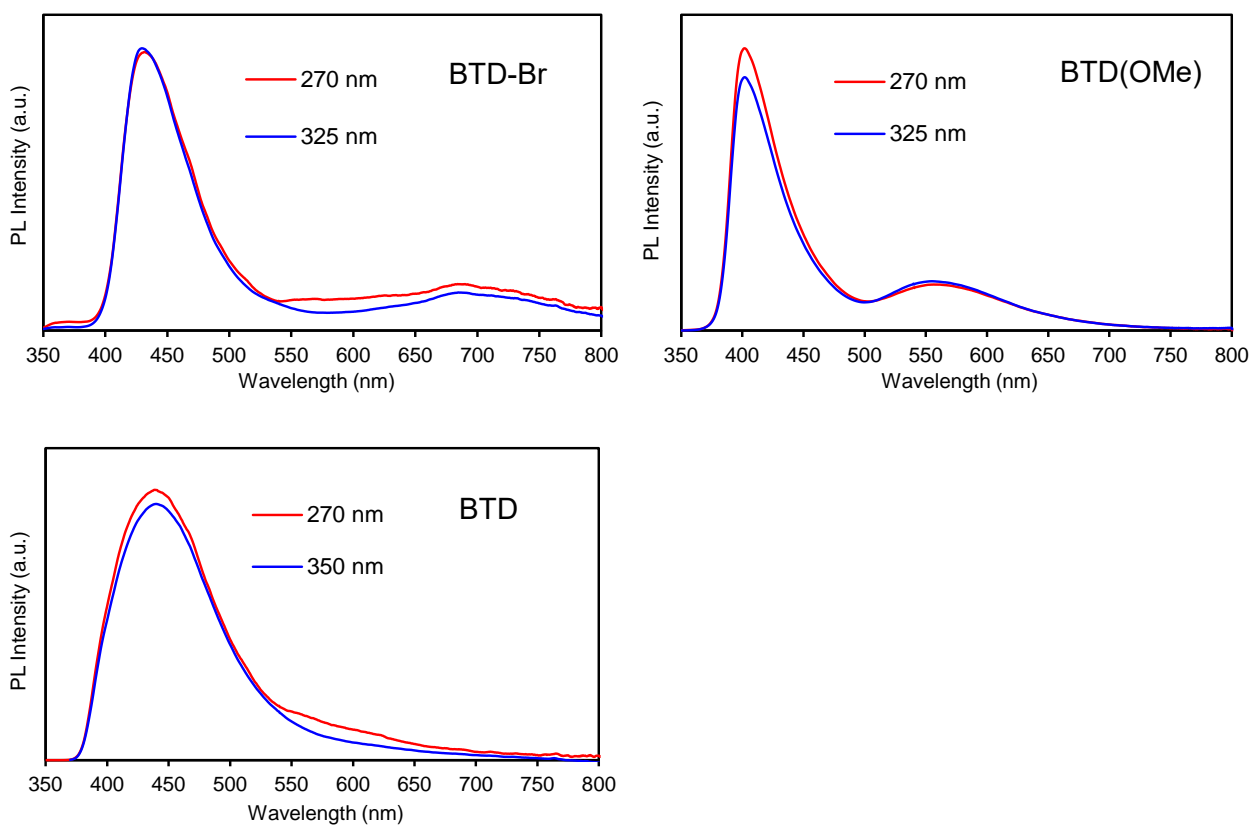


Fig. S11 Excitation dependence of steady-state photoluminescence spectra (excited at 270 and 325 nm) of BTD-Br, BTD(OMe), and BTD in the crystalline solid state.

These weakly phosphorescent dyes BTD-Br, BTD(OMe), and BTD did not show the significant excitation dependence.

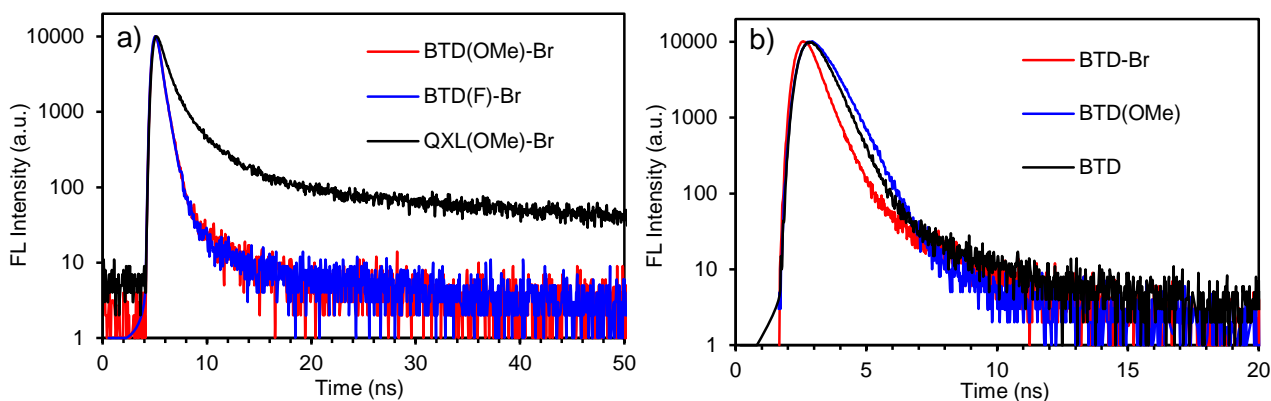


Fig. S12 Fluorescence decay curves of (a) BTD(OMe)-Br, BTD(F)-Br, and QXL(OMe)-Br (monitored at 450, 420, and 420 nm, respectively) and (b) BTD-Br, BTD(OMe), and BTD (monitored at 420 nm). Experimental decay curves are fitted with a double- or triple-exponential function.

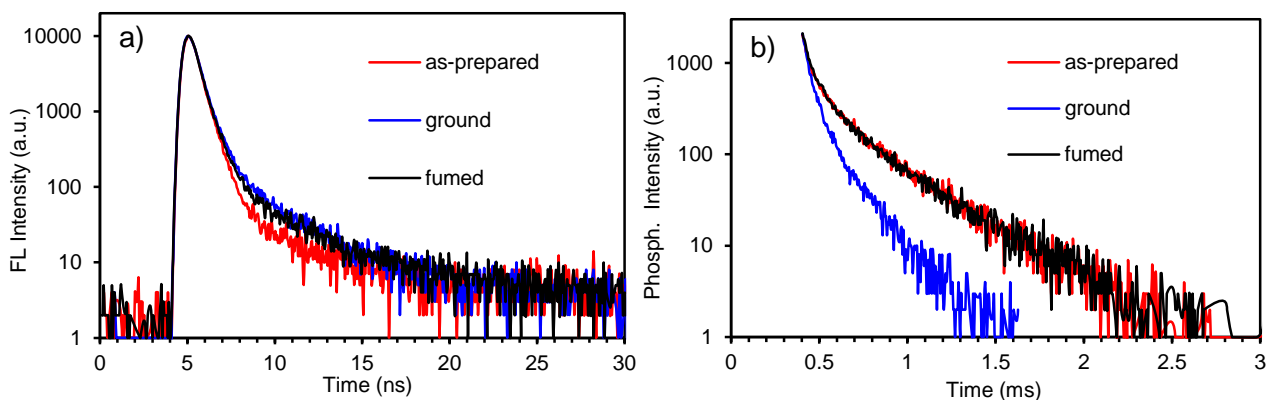


Fig. S13 (a) Fluorescence and (b) phosphorescence decay curves of BTD(OMe)-Br in the as-prepared, ground, and fumed (chloroform-vapor) state at fluorescence and phosphorescence maxima (450 and 640 nm) with excitation at 340 nm. Experimental decay curves are fitted with a double- or triple-exponential function.

Table S2 Spectral data of benzothiadiazole-based dyes in the crystalline solid state

Comp.	λ_{abs} (nm)	Fluorescence ^a				Phosphorescence ^a				
		λ_{F} (nm)	Φ_{F} (%) ^b	τ_{F} (ns) (f_{i} (%)) ^c	$\langle \tau_{\text{F}} \rangle$ (ns) ^d	λ_{P} (nm)	Φ_{P} (%) ^b	τ_{P} (μs) (f_{i} (%)) ^c	$\langle \tau_{\text{P}} \rangle$ (μs) ^d	
BTD(OMe)-Br (as-prepared)	403	448	0.4	0.10 (98)	2.32	648	3.7	17.2 (8)	585	
	295(sh)			4.58 (2)			6.9 ^e	143.2 (31)		
	260(sh)							636.6 (61)		
	220(sh)									
	(ground)	391	445	0.4	0.05 (90)	4.11	645	1.9	10.0 (8)	264
		295(sh)			4.51 (10)				80.9 (48)	
		263							316.4 (44)	
		219								
	(fumed)	401	446	0.4	0.04 (96)	3.79	648	3.7	16.9 (7)	591
		295(sh)			4.66 (4)				140.5 (36)	
		260(sh)							654.0 (57)	
		220(sh)								
(77 K)	–	482	0.7	–	–	650	6.5	–	–	
		455				610(sh)				
		425(sh)								
(PMMA film)	375(sh)	425	–	–	–	642	–	–	–	
	324									
	215									
BTD(F)-Br	382	422	0.4	0.1 (97)	2.34	629	1.8	2.4 (8)	233	
	295(sh)			4.37 (3)			2.4 ^e	58.4 (63)		
	260(sh)							306 (29)		
	215(sh)									
	(77 K)	–	435	0.8	–	–	670	3.3	–	–
		417				650				
						623				
QXL(OMe)-Br	370	426	0.1	0.12 (47)	23.1	600(sh)	1.6	6.1 (13)	110	
	295(sh)			1.93 (33)		559	3.3 ^e	34.7 (44)		
	260(sh)			26.0 (20)		525(sh)		132 (43)		
	215(sh)									
	(77 K)	–	462	0.1	–	–	594	4.2	–	–
						558				
BTD-Br	387	430	0.5	0.10 (98)	0.84	685	0.1	1.1 (45)	37	
	340(sh)			2.25 (2)				5.1 (31)		
	295(sh)							43.8 (24)		
	260(sh)									

	215(sh)								
BTD(OMe)	369	402	2.3	0.12 (26)	0.48	555	0.5	0.6 (27)	73
				0.51 (74)				28.8 (26)	
							81.9 (47)		
	215(sh)								
BTD	367	440	1.2	0.27 (97)	0.49	–	–	–	–
				1.66 (3)					
	217								

^a Excited at 325 nm, ^b Absolute fluorescence and phosphorescence quantum yields determined by an integrating sphere system, ^c The value in parentheses is the fractional contribution of component i to the total steady-state intensity, which was calculated by $f_i = (A_i \tau_{Fi} / \sum A_i \tau_{Fi}) \times 100$, ^d The intensity-averaged decay lifetime ($\langle \tau \rangle$) was calculated as follows: $\langle \tau \rangle = \sum (A_n \tau_n^2) / \sum (A_n \tau_n)$, in which A_n is the coefficient of each exponential term, ^e Excited at 270 nm.

Table S3 Fluorescence and phosphorescence quantum yields of benzothiadiazole-based dyes in the crystalline solid state

Comp.	Conditions	Ex. (nm)	Φ_F (%) ^a	Φ_P (%) ^a
BTD(OMe)-Br	as-prepared	270	0.4	6.9
		300	0.4	4.4
		325	0.4	3.7
		350	0.4	3.0
		380	0.4	2.9
	ground	270	0.4	2.6
		300	0.4	2.1
		325	0.4	1.9
		350	0.4	1.6
	fumed	270	0.4	6.7
300		0.4	4.3	
325		0.4	3.7	
350		0.4	3.0	
BTD(F)-Br	as-prepared	270	0.4	2.4
		300	0.4	2.0
		325	0.4	1.8
		350	0.4	1.7
QXL(OMe)-Br	as-prepared	270	0.1	3.3
		300	0.1	2.5
		325	0.1	1.6
		350	0.1	1.5
BTD-Br	as-prepared	270	0.5	0.1
		325	0.5	0.1
BTD(OMe)	as-prepared	270	2.4	0.5
		325	2.3	0.5
BTD	as-prepared	270	1.2	–
		325	1.2	–

^a Absolute fluorescence and phosphorescence quantum yields determined by an integrating sphere system.

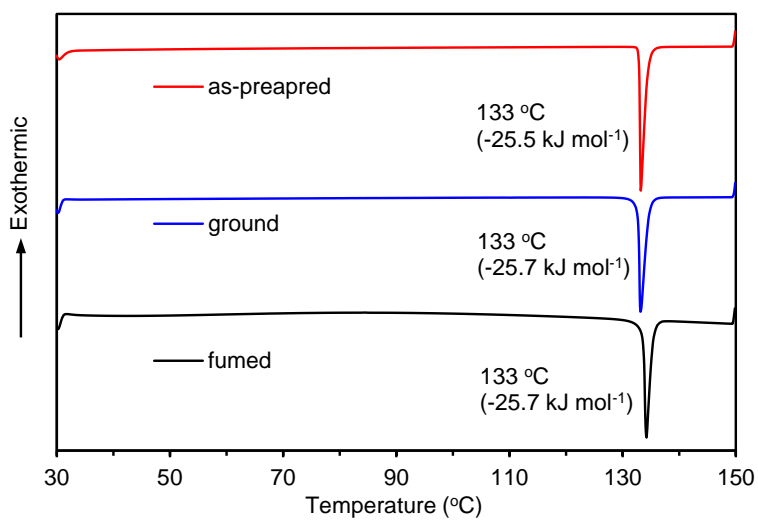


Fig. S14 DSC curves of BTD(OMe)-Br in the as-prepared, ground, and fumed (chloroform-vapor) state. The value in parenthesis is the enthalpy value of melting point.

An endothermic peak at 133 °C corresponding to the melting point exhibited little change before and after mechanical grinding. Probably, the crystal packing structure did not change at the macroscopic level.

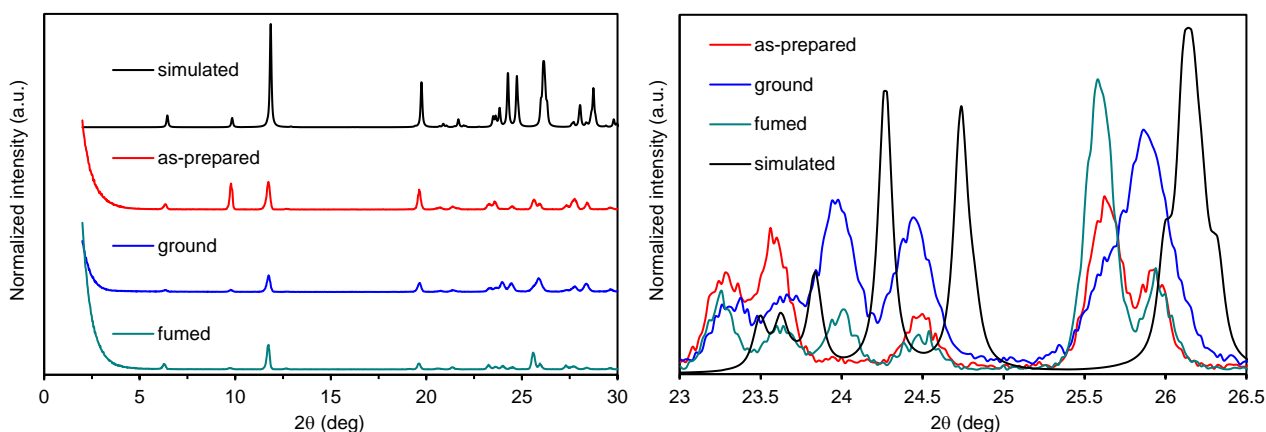


Fig. S15 Powder XRD patterns of BTD(OMe)-Br in the as-prepared, ground, and fumed (chloroform-vapor) state, and the simulated powder pattern of the as-prepared sample derived from a single crystal. The right figure is an expansion in the 2θ range of $23\text{--}26.5^\circ$.

A slight change of diffraction peaks was observed in the wide angle region ($23\text{--}26.5^\circ$), corresponding to $\pi\cdots\pi$, $\text{C-H}\cdots\text{O}$, and $\text{Br}\cdots\text{Br}$ contacts. Probably, a trace amounts of defects was formed in the microscopic crystal packing upon mechanical grinding, resulting in the slightly reduced phosphorescence.

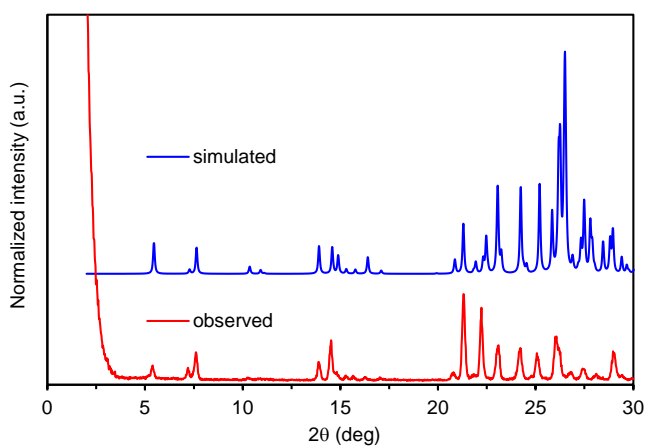


Fig. S16 Powder XRD pattern of BTD(F)-Br in the crystalline solid state and the simulated powder pattern derived from a single crystal.

Computer simulation analysis.

All quantum chemical calculations based on the time-dependent density functional theory (TD-DFT) were performed using the ADF2019 program package.¹ The ground-state (S_0) geometries for the compound BTD(OMe)-Br were initially optimized using the B3LYP functional with the DZP basis set in the gas phase. The vertical excitation calculations were carried out using the optimized S_0 geometries, and the geometry optimizations in the excited S_1 and T_1 states were performed using TD-DFT at the same level of theory. For the $S_0 \rightarrow S_m$ ($m = 1-4$) and $S_0 \rightarrow T_n$ ($n = 1-4$) transitions, the natural transition orbitals (NTOs) with their excitation energies were simulated using the optimized S_1 and T_1 geometries, respectively. Using the T_1 geometries, the spin-orbit coupling matrix elements, $\langle S_m | \hat{H}_{\text{SOC}} | T_n \rangle$, were calculated using a scalar relativistic TD-DFT with the two-component zeroth-order relativistic approximation (ZORA)² at the same level of theory. The contributions of the three degenerate triplet states ($T_{n,x}$, $T_{n,y}$, and $T_{n,z}$) were taken into account by calculating the root sum square of the real and imaginary parts (Re and Im, respectively) of the matrix elements, as expressed by the following equation:³

$$\langle S_m | \hat{H}_{\text{SOC}} | T_n \rangle = \left\{ \sum_{a=x,y,z} (\text{Re}^2 \langle S_m | \hat{H}_{\text{SOC}} | T_{n,a} \rangle + \text{Im}^2 \langle S_m | \hat{H}_{\text{SOC}} | T_{n,a} \rangle) \right\}^{1/2}$$

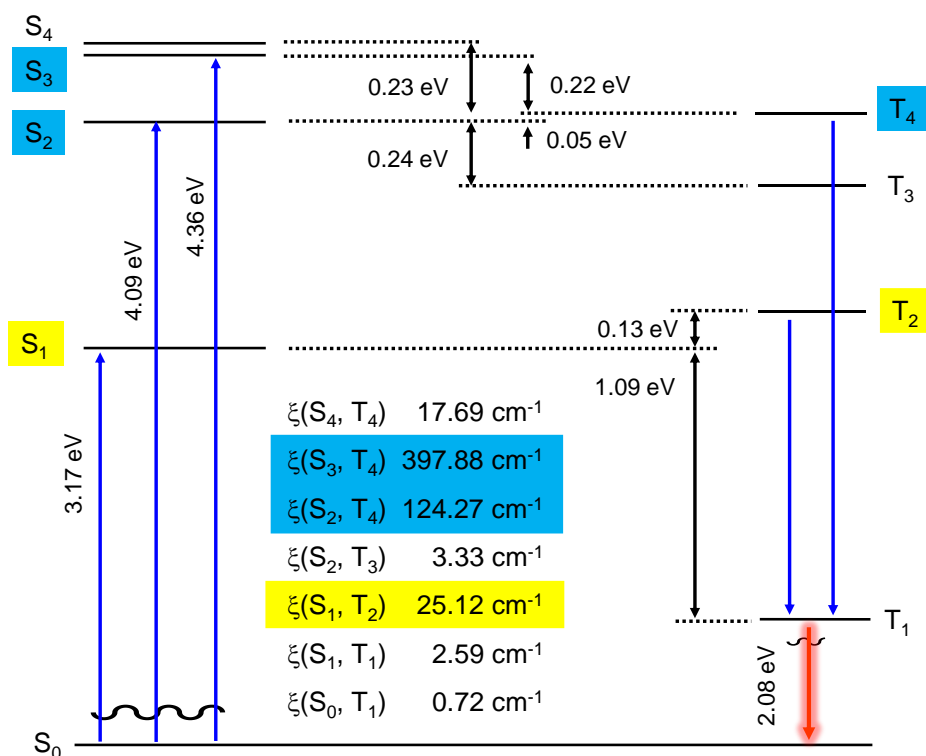


Fig. S17 Theoretical calculated energy diagram and spin-orbit coupling (ξ) of BTD(OMe)-Br.

A favored intersystem crossing in S_2/T_4 and S_3/T_4 was indicated by higher SOC values of 124.27 and 397.88 cm^{-1} , respectively, together with small band gap within 0.22 eV. Although in the S_1/T_2 intersystem crossing the SOC value of 25.12 cm^{-1} is smaller than those in S_2/T_4 and S_3/T_4 , the value is enough large compared with the SOC values reported in organic phosphorescent dyes.⁴ The large energy gap (>0.92 eV) between S_1 and S_2 (or S_3) is supportive of the intersystem crossing starting from higher-lying S_2 (or S_3), because the internal conversion from S_2 (or S_3) to S_1 is slow.

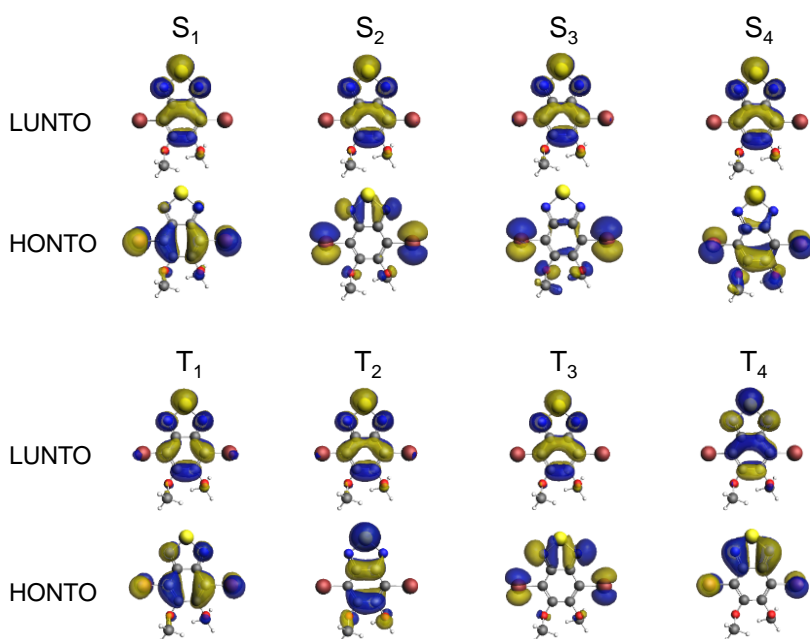


Fig. S18 Theoretical calculated natural transition orbitals (HNTOs and LNTOs) of BTD(OMe)-Br.

According to El-Sayed rule, the S_1/T_2 intersystem crossing is unfavored, because both the S_1 and T_2 states can be assigned to the same configuration of π/π^* transition. In contrast, the intersystem crossing in S_2/T_4 and S_3/T_4 is likely to be favored because of the contribution of both π/π^* and n/π^* configurations.

1 ADF2019, SCM, Theoretical Chemistry, Vrije Universiteit, Amsterdam, The Netherlands,
<http://www.scm.com/>.

2 F. Wang and T. Ziegler, *J. Chem. Phys.*, 2005, **123**, 154102.

3 E. Y.-T. Li, T.-Y. Jiang, Y. Chi and P.-T. Chou, *Phys. Chem. Chem. Phys.*, 2014, **16**, 26184–26192.

4 H. Shi, L. Zou, K. Huang, H. Wang, C. Sun, S. Wang, H. Ma, Y. He, J. Wang, H. Yu, W. Yao, Z. An, Q. Zhao and W. Huang, *ACS Appl. Mater. Interfaces*, 2019, **11**, 18103–18110.

Single crystal X-ray diffraction analysis.

The single crystals for the X-ray diffraction analysis were obtained by the slow diffusion of hexane into the chloroform solution in BTD(OMe)-Br (colorless needles) and by heating of hexane suspension and subsequent cooling to room temperature in BTD(F)-Br (colorless needles).

All measurements were made on a Rigaku HyPix-6000 HE diffractometer using multi-layer mirror monochromated Mo-K α radiation. Using Olex2,¹ the structure was solved with the Olex2.solve² structure solution program using Charge Flipping and refined with the Olex2.refine² refinement package using Gauss-Newton minimization. The non-hydrogen atoms were refined anisotropically. Hydrogen atoms were refined using the riding model. Simulated powder patterns were generated with Mercury 4.2 from the structures determined by single crystal diffraction analyses.³

1 O. V. Dolomanov, L. J. Bourhis, R. J. Gildea, J. A. K. Howard and H. Puschmann, OLEX2: A complete structure solution, refinement and analysis program. *J. Appl. Cryst.*, 2009, **42**, 339–341.

2 L. J. Bourhis, O. V. Dolomanov, R. J. Gildea, J. A. K. Howard and H. Puschmann, *Acta Cryst.*, 2015, **A71**, 59–75.

3 <https://www.ccdc.cam.ac.uk/support-and-resources/Downloads/>

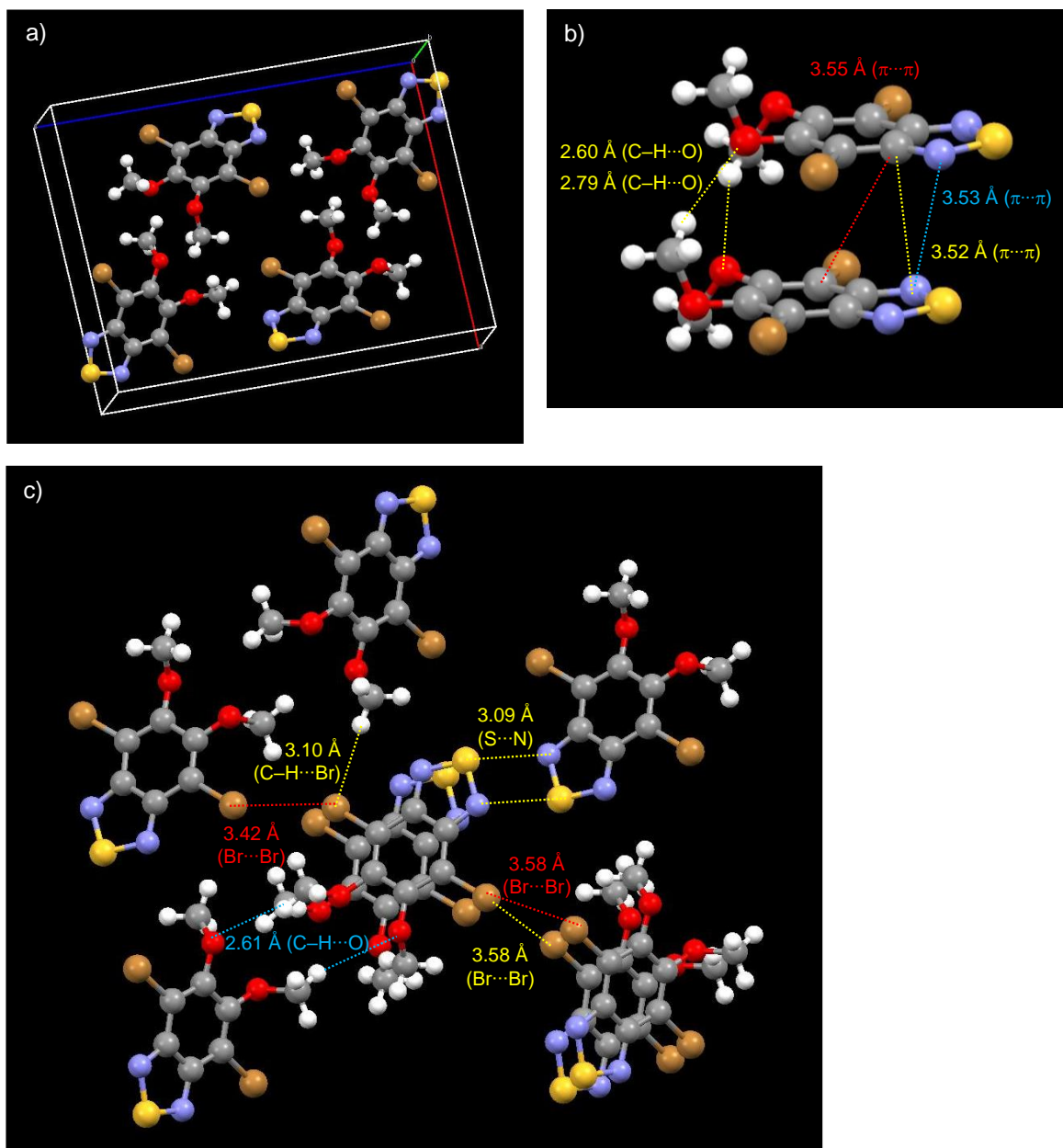


Fig. S19 Single crystal X-ray structure of BTDO(OMe)-Br: a) unit cell packing, b) dimeric structure in the one-dimensional columnar structure (shown in Fig. 5a in the manuscript), and c) intermolecular non-bonded interactions around the dimeric structure (shown in Fig. S19b).

The dimeric structure constructed by $\pi \cdots \pi$ stacking interactions is assisted by the two-point C–H \cdots O interactions. The inter-columnar structure is stabilized by the multiple non-bonded interactions including halogen interactions, leading to an acceleration of ISC and the subsequent stabilization of excited triplet state.

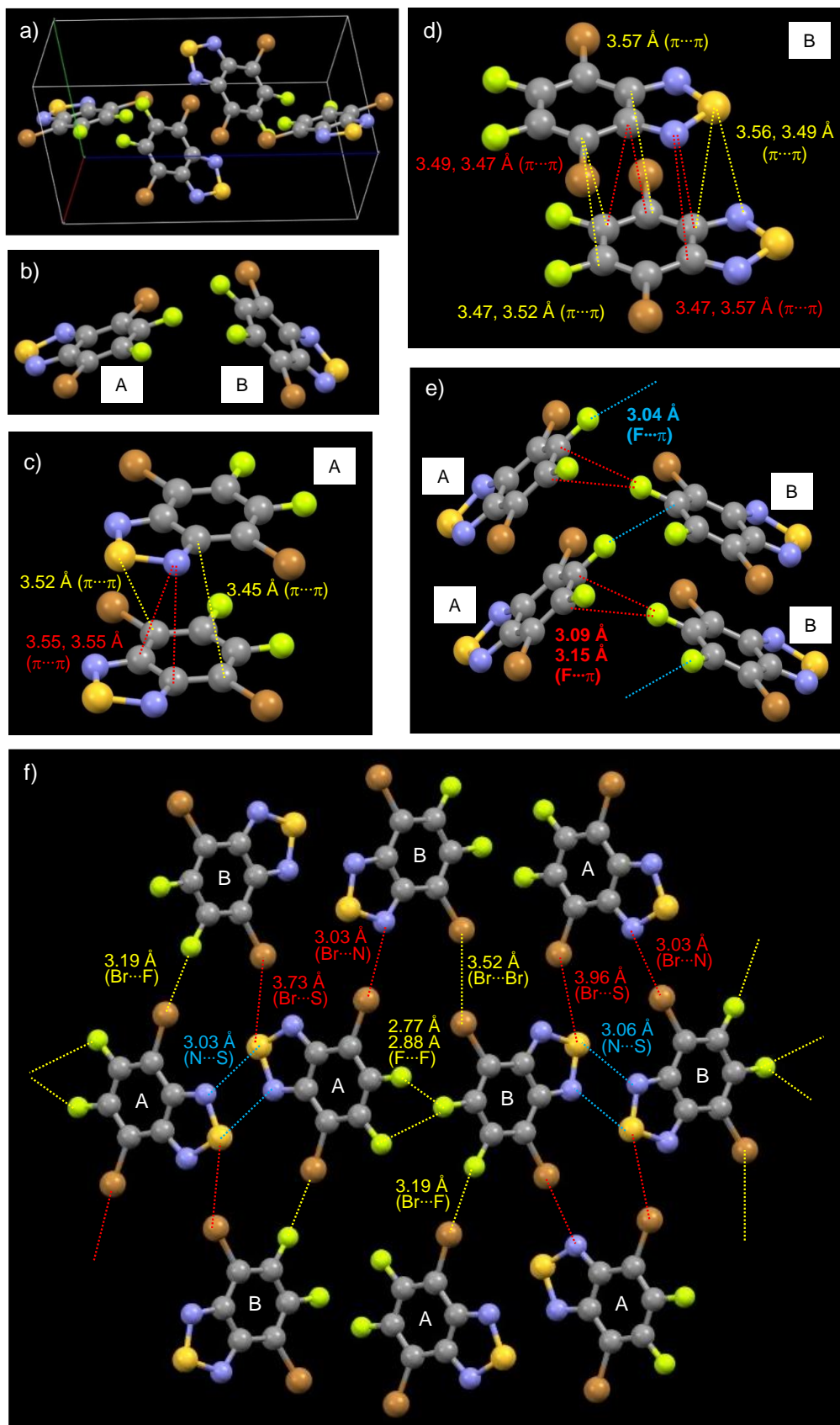


Fig. S20 Single crystal X-ray structure of BTDF(Br)-Br: a) unit cell packing, b) two independent molecules A and B, c) and d) dimeric structures of A and B molecules in the one-dimensional columnar structures (shown in Fig. 5b in the manuscript), e) intermolecular non-bonded interactions between the two dimeric structures

(shown in Fig. 20c and 20d), and d) intermolecular non-bonded interactions among A and B molecules.

The inter-columnar structure is stabilized by the multiple non-bonded interactions including halogen interactions, leading to an acceleration of ISC and the subsequent stabilization of excited triplet state.

Table S4 Selected data for the single crystals of BTD(OMe)-Br and BTD(F)-Br dyes.

data		BTD(OMe)	BTD(F)-Br
Monomer:			
molecular symmetry		asymmetry	symmetry
independent molecules		–	two independent molecules (A and B)
bond length (Å)	C–Br	1.874, 1.874	A: 1.864, 1.866 B: 1.872, 1.872
	C–O	1.363, 1.369	–
	C–F	–	A: 1.329, 1.338 B: 1.328, 1.339
dihedral angle (°)	BTd–OMe	85.3, 101.1	–
Stacked dimer:			
intermolecular interactions (Å)	BTd⋯BTd ($\pi\cdots\pi$)	3.518, 3.528, 3.553,	A: 3.449, 3.518, 3.549, 3.553 B: 3.467, 3.468, 3.470, 3.489, 3.494, 3.515, 3.556, 3.568, 3.572
(torsion angle (°))	OMe⋯OMe (C–H⋯O)	2.600 (149.5°), 2.786 (161.9°)	
Packing:			
intermolecular interactions (Å)	Br interactions	3.416 (Br⋯Br), 3.575 (Br⋯Br), 3.575 (Br⋯Br),	3.521 (Br⋯Br), 3.194 (Br⋯F), 3.029 (Br⋯N),
(torsion angle (°))		3.103 (146.1°) (C–H⋯Br),	3.034 (Br⋯N), 3.725 (Br⋯S), 3.958 (Br⋯S)
	N/S interactions	3.089 (N⋯S)	3.025, 3.057 (N⋯S)
	F interactions		2.773, 2.875 (F⋯F) 3.040 (158.18°), 3.086 (153.04°), 3.147 (163.46°) (C–F⋯ π)
	others	2.612 (164.4°) (C–H⋯O)	

Table S5 Crystallographic data for BTD(OMe)-Br and BTD(F)-Br dyes.

	BTD(OMe)-Br	BTD(F)-Br
CCDC number	2234914	2234915
formula	C ₈ H ₆ Br ₂ N ₂ O ₂ S	C ₆ Br ₂ F ₂ N ₂ S
M	354.03	329.96
<i>T</i> [K]	100	100
crystal system	monoclinic	triclinic
space group	<i>P</i> 2 ₁ / <i>c</i> (no. 14)	<i>P</i> ₋₁ (no. 2)
<i>a</i> [Å]	13.7002 (7)	4.0701 (2)
<i>b</i> [Å]	4.3371 (2)	12.7597 (6)
<i>c</i> [Å]	17.9709 (8)	17.0263 (9)
α [°]	90	72.084 (4)
β [°]	90.883 (4)	89.411 (4)
γ [°]	90	89.426 (4)
<i>V</i> [Å ³]	1067.69 (9)	841.29 (7)
<i>Z</i>	4	4
ρ_{calcd} [g cm ⁻³]	2.202	2.605
μ [mm ⁻¹]	7.767	9.863
	$\mu(\text{MoK}\alpha)$	$\mu(\text{MoK}\alpha)$
<i>F</i> (000)	680	616
crystal size [mm ³]	0.3 × 0.1 × 0.02	0.22 × 0.02 × 0.01
θ range [°]	2.27–27.5	2.39–27.75
index range	–16 17	–5 5
	–5 5	–16 16
	–22 23	–22 22
reflections collected	8878	3887
reflections unique	2420	3887
<i>R</i> _{int}	0.0427	0.051
data [<i>F</i> ² > 2σ (<i>F</i> ²)]	2170	3438
parameters	138	236
goodness-of-fit	1.074	1.252
<i>R</i> 1/ <i>wR</i> ² [<i>F</i> ² > 2σ (<i>F</i> ²)]	0.0303/0.0696	0.0516/0.1621
<i>R</i> 1/ <i>wR</i> ² (all data)	0.0361/0.0718	0.0610/0.1655
Resd. min/max [eÅ ⁻³]	–0.71/0.78	–1.39/1.67
Max Shift/error in final cycle	0.001	0.000

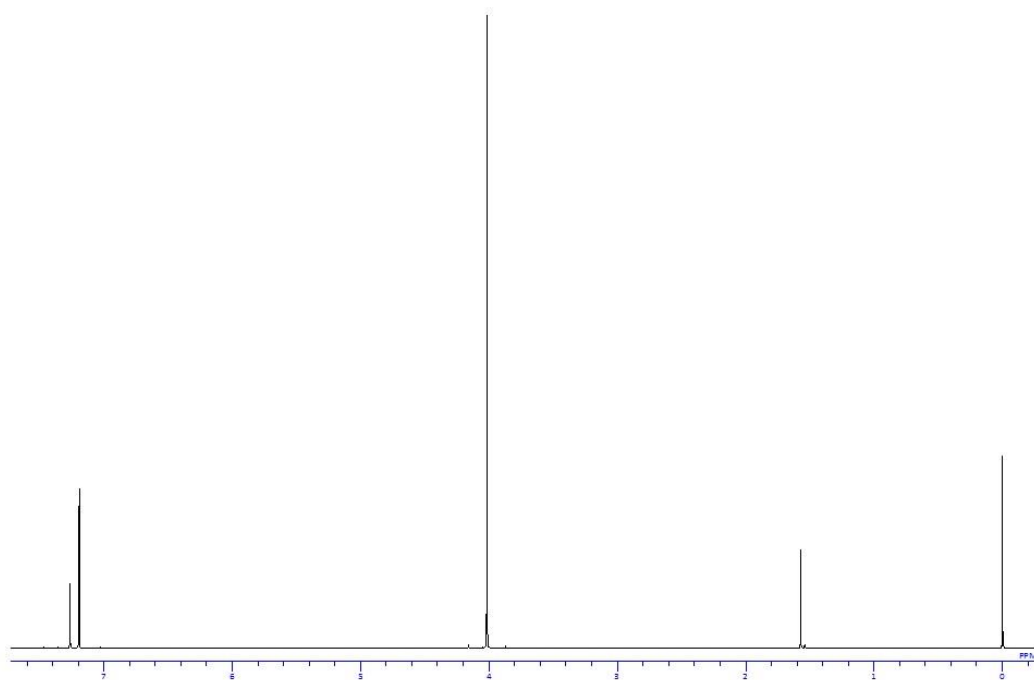


Fig. S21 ¹H NMR spectrum of BTD(OMe) in CDCl₃ at room temperature.

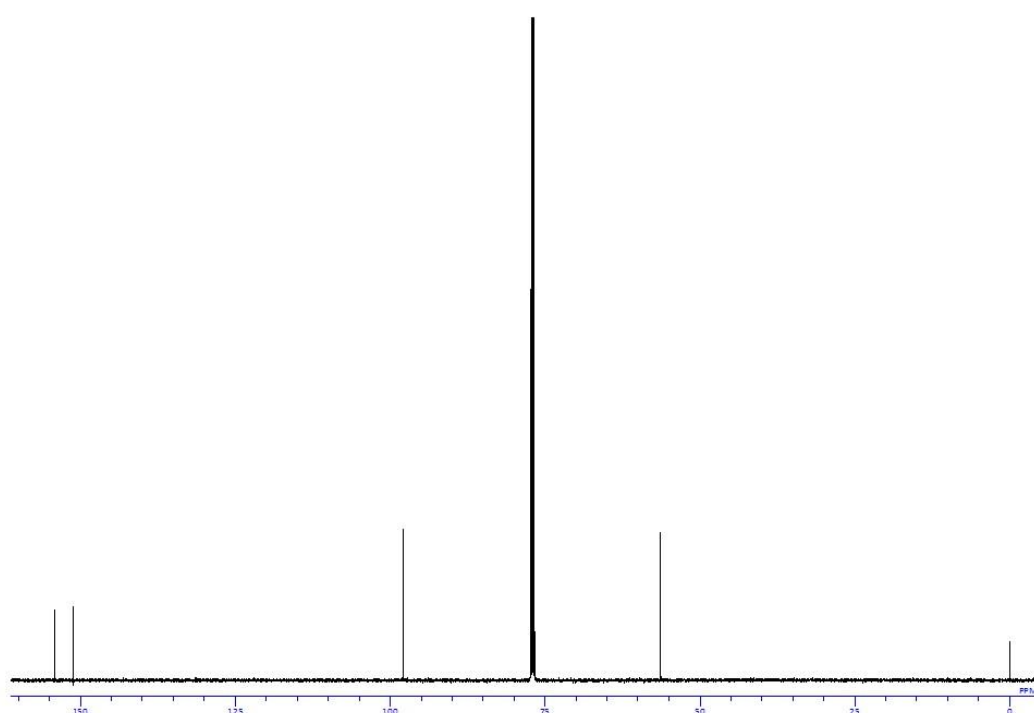
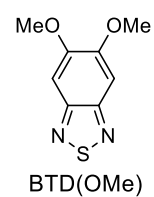


Fig. S22 ¹³C NMR spectrum of BTD(OMe) in CDCl₃ at room temperature.

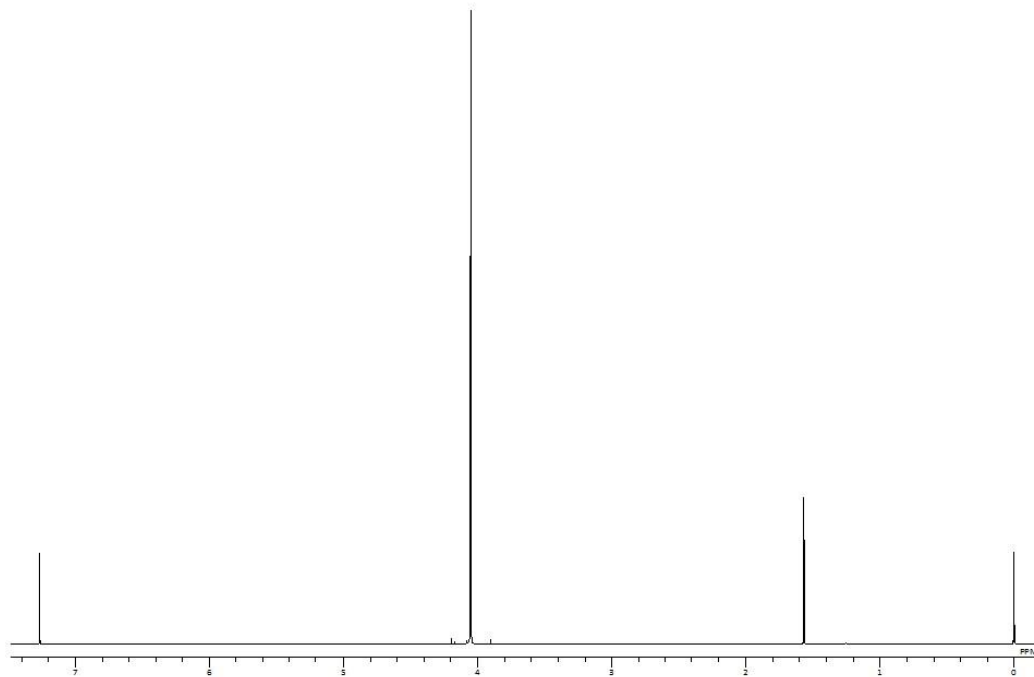


Fig. S23 ^1H NMR spectrum of BTD(OMe)-Br in CDCl_3 at room temperature.

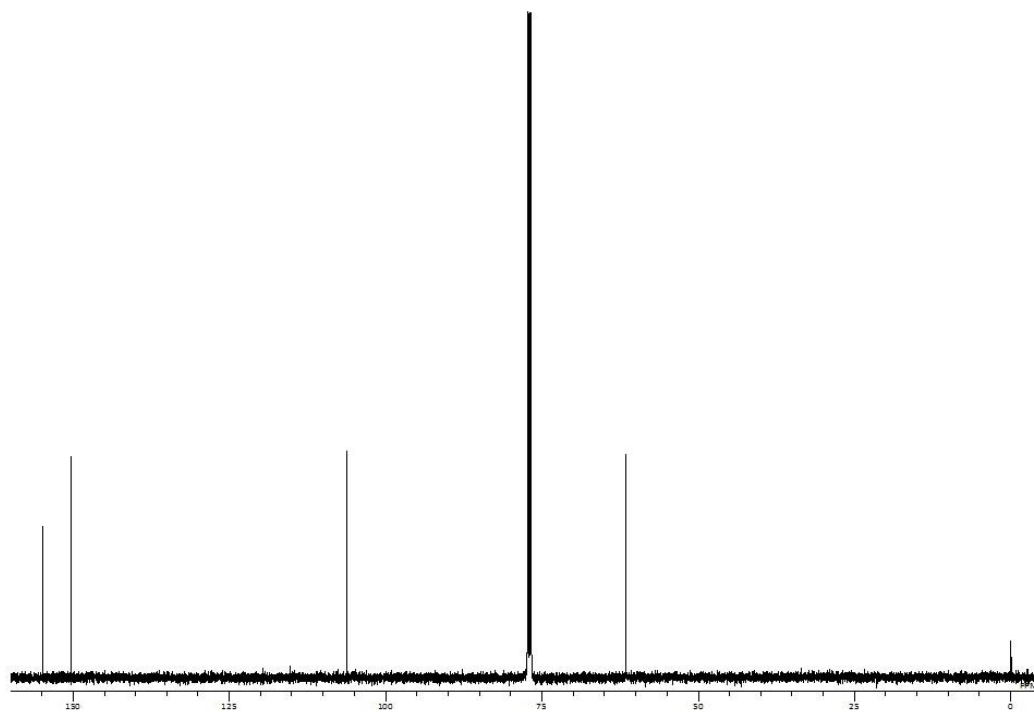


Fig. S24 ^{13}C NMR spectrum of BTD(OMe)-Br in CDCl_3 at room temperature.

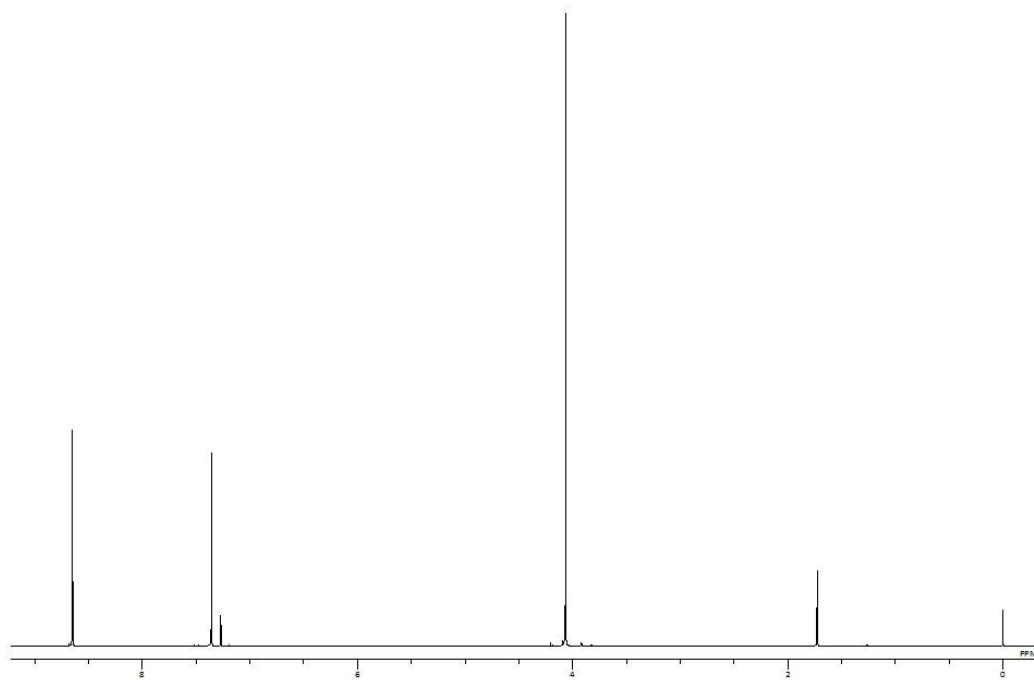


Fig. S25 ^1H NMR spectrum of **2** in CDCl_3 at room temperature.

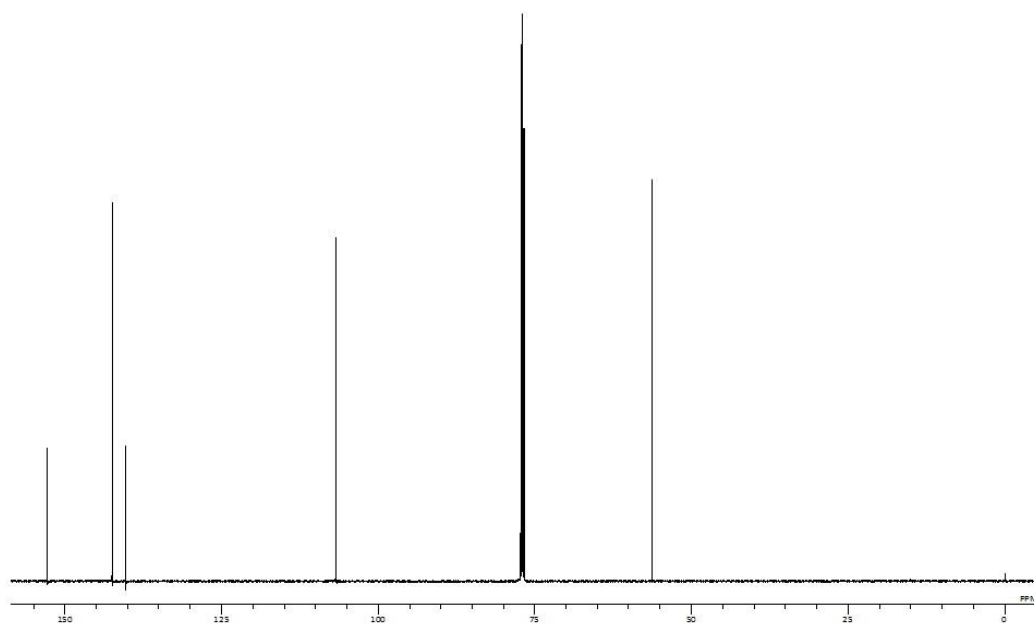
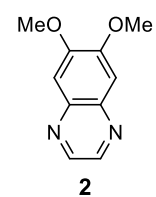


Fig. S26 ^{13}C NMR spectrum of **2** in CDCl_3 at room temperature.

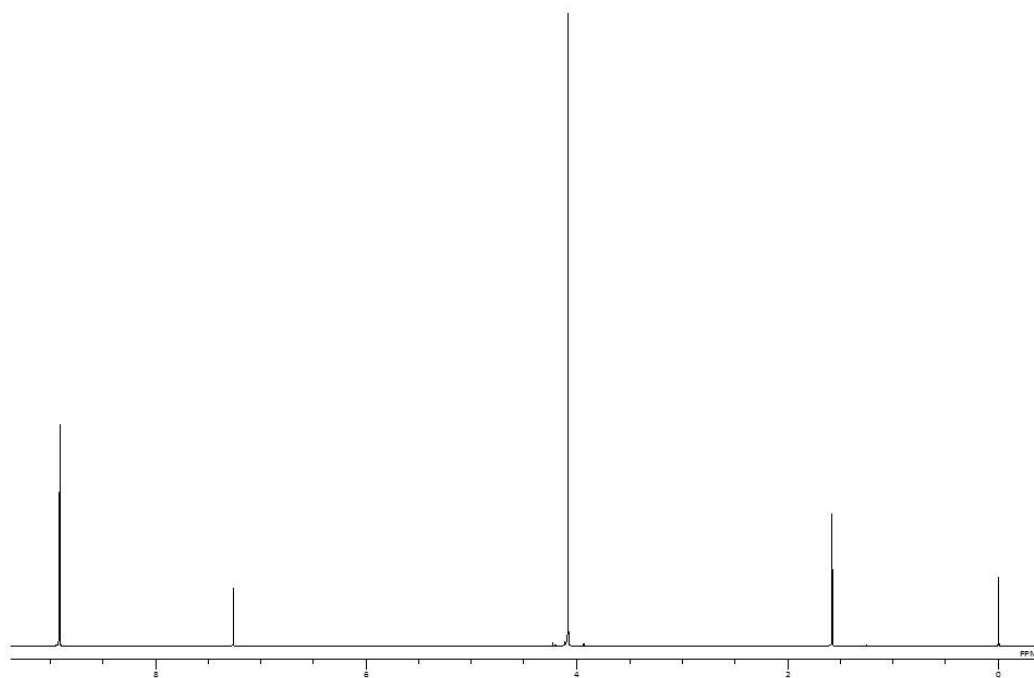


Fig. S27 ^1H NMR spectrum of QXL(OMe)-Br in CDCl_3 at room temperature.

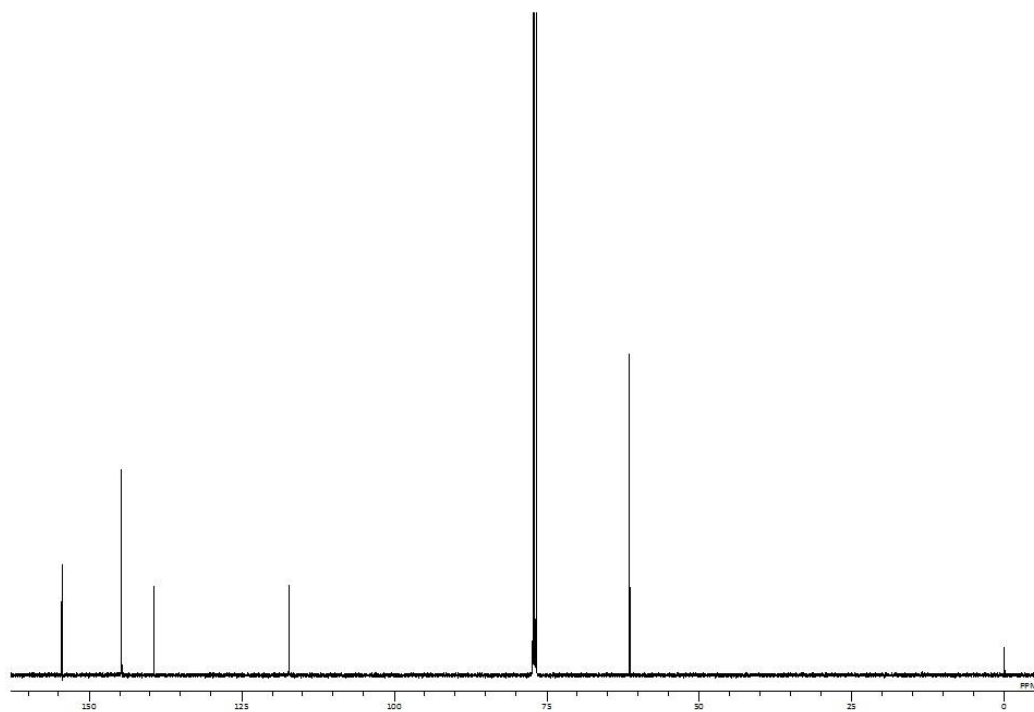
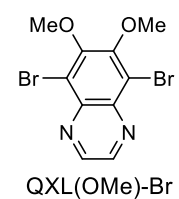


Fig. S28 ^{13}C NMR spectrum of QXL(OMe)-Br in CDCl_3 at room temperature.